Connecting Plate Boundary Processes to Earthquake Faults using Geodetic and Topographic Imaging

Andrea Donnellan[1], Ramón Arrowsmith[2], Yehuda Ben-Zion[3], John Rundle[4], Lisa Grant Ludwig[5], Margaret Glasscoe[1], Adnan Ansar[1], Joseph Green[1], Jay Parker[1], John Pearson[1], Cathleen Jones[1], Paul Lundgren[1], Stephen DeLong[6], Taimi Mulder[7], Eric De Jong[1], William Hammond[8], Klaus Reicherter[9], Ted Scambos[10]

[1]Jet Propulsion Laboratory, California Institute of Technology, [2]Arizona State University, [3]University of Southern California, [4]University of California Davis, [5]University of California, Irvine, [6]US Geological Survey, [7]Pacific Geoscience Center, Natural Resources Canada, [8]University of Nevada, Reno, [9]RWTH Aachen University, [10]National Snow and Ice Data Center

Large earthquakes cause billions of dollars in damage and extensive loss of life and property. Losses are escalating due to increasing urbanization near plate boundaries and aging buildings and infrastructure. Earthquakes occur when accumulated stress from plate tectonic motions exceeds the strength of faults within the Earth's crust. Stress in the Earth's crust and lithosphere cannot be measured directly, but stress conditions and fault properties can be inferred from seismology, measurement of surface deformation, and topography.

Remote sensing from air or space provides measurements of transient and long-term crustal deformation, which are needed to improve our understanding of earthquake processes. While our main focus is on topographic imaging, geodetic imaging provides the necessary context of present-day crustal deformation. We advocate for continued GPS and InSAR crustal deformation measurements from the existing global geodetic network, the Plate Boundary Observatory, international Interferometric Synthetic Aperture Radar (InSAR) satellites, NASA's airborne UAVSAR platform, and NASA/ISRO's planned NISAR mission. Topographic imaging of long-term and episodic motions on scales of days to years is necessary and complements crustal deformation measurements. Lidar as well as structure from motion from multi-angle imaging of a target produce 3D point clouds. Fixed-point multi-angle staring imaging can also produce color draped topographic images. This white paper recommends topographic imaging in the necessary context of geodetic crustal deformation measurements and complements a white paper submitted to the first decadal survey request for information (Donnellan et al, 2014).

Understanding the Spatio-Temporal Behavior of Faults Is Key to Mitigating Earthquake Hazard

Science and Application Target: *Earth Surface and Interior: Dynamics and Hazards*

Earthquakes accommodate driving motions of the tectonic plates. Plate boundaries consist of broad zones of deformation typically made up of complicated networks of faults at the surface (Figure 1). Strain accumulates from differential plate motions until the crust eventually fails along fault boundaries. Some fraction of that strain is released aseismically as silent slip along faults or as bulk deformation within the Earth's crust while the rest is seismic and therefore potentially damaging. It is possible to infer how the surface fault network connects and cuts crustal material by combining seismological observations with measurement of topography and the distribution of strain across the plate boundary. Space-based measurements are ideally suited to provide a synoptic view of plate boundary deformation.

Knowledge of the amount of aseismic versus seismic deformation is key to earthquake hazard assessment. Fault offsets and deformation from individual earthquakes accumulate to create landforms that are records of permanent deformation. Over time erosion modifies and reshapes these landforms. Major earthquakes may occur infrequently along any particular fault, but over the global tectonic system they occur dozens of times per year.

NASA's 2016 report *Challenges and Opportunities for Research in Earth Surface and Interior (CORE)* asks seven questions, at least three of which are relevant to this white paper (Davis et al, 2016):

1. *What is the nature of deformation from plate boundaries and what are the implications for earthquakes, tsunamis, and other related natural hazards?*
2. *How do tectonic processes and climate variability interact to shape the Earth's surface and create natural hazards?*
3. *What are the dynamics of the Earth's deep interior and how does the Earth's surface respond?*

Surface motions reflect deeper crustal deformation at plate boundaries. The zone of deformation between two tectonic plates can be 100s of km wide and 1000s of km long. Complex fault networks form the boundaries of tectonic plates. Fault zones develop and change as earthquakes repeatedly accommodate relative plate motion. Surface processes driven by gravity, flowing water, and biological systems modify fault zones further. Tectonic motion and erosion may operate together creating rock damage and landscape asymmetry across faults. The landscape provides information about fault offsets, stress directions, and rupture characteristics (Figure 2).

Landscape asymmetry is likely a reflection of compositional and mechanical asymmetry in the Earth's crust (Wechsler et al, 2009; Dor et al., 2008). This is critically important because earthquakes tend to rupture in the direction of slip on the more compliant side of the fault (Ben-Zion and Shi, 2005). Rupture directivity can have a large impact on damage. If the southern San Andreas fault were to rupture from south to north, the directivity combined with basin waveguide effects would produce unusually high long-period ground motions near Los Angeles with intense localized amplitude modulations (Olsen et al, 2006). Conversely, the damage is likely to be far greater in the Coachella valley and south of the US-Mexico border if the fault were to rupture from north to south. Characterizing landscape asymmetry across large faults will provide key input on possible existence of preferred rupture directivity at different fault sections, which can improve seismic hazard assessments in large metropolitan areas.

Geodetic and topographic imaging observations from space can address the following questions:

- How do plate boundary motions connect to surface faults and their associated deformation?
- How does plate deformation partition between seismic and aseismic release and what are the implications for earthquake hazards?
- How do faults rupture and slip throughout multiple earthquake cycles and what are the implications for earthquake hazard?

Faults collectively accommodate strain across large plate boundary systems, connecting in complicated ways that vary with depth and tectonic environment. In some cases, adjacent faults do not explicitly connect at all, indicating that some strain may be accommodated aseismically. This is especially the case off the main plate boundary faults in California and Cascadia. For example, in the Intermountain Western United States thousands of faults (e.g. Wesnousky, 2005; dePolo, 2008) accommodate 25% of the total plate motion and are potential earthquake sources (e.g. Dokka and Travis, 1990; Thatcher et al, 1999).

The width of the tectonic boundary can be determined from measurement of crustal deformation, particularly from high-precision GPS networks. A combination of measurement of surface morphology and crustal deformation can help determine the role of a ductile lower crust in transferring strain to the upper crust. Detailed measurement of fault zone morphology will provide information on how fault systems evolve and mature over time.

Both geodetic and topographic measurements can be used to measure coseismic and postseismic motions from earthquakes. Comparison of detailed measurements of seismicity and coseismic strain to the long periods of interseismic motion are currently the only method

available for determining how much of the accumulated strain may be aseismically released. Topographic imaging methods fill a particularly important gap near fault ruptures where InSAR observations tend to decorrelate. Furthermore, at high spatial resolution the topography contains dense geodetic markers, and topographic imaging provides advantages over InSAR in rugged terrain with no layover correction, and no shadowing. Comparison of detailed measurements of seismicity and coseismic strain to the long periods of interseismic motion are currently the only method available for determining how much of the accumulated strain may be aseismically released. The 2014 M6.0 South Napa earthquake was observed with UAVSAR, NASA's airborne InSAR instrument; however, the radar decorrelated between the before and after pair of images, leaving a 4km wide and 15km long observational gap near the rupture (Figure 3). The earthquake ruptured a scarp identifiable in lidar imagery from before the earthquake but 5 km west of the fault trace previously mapped as most active (DeLong et al, submitted). Pre- and post-earthquake topographic imaging are essential to reveal in 3D how complex rupture patterns accommodate moment release during earthquakes and constrains the distribution of damaging post-seismic deformation.

Measuring Transient and Permanent Deformation using Geodetic and Topographic Imaging

Utility of Targeted Geophysical Variable: *Assessing Earthquake Hazard*

Annualized losses from earthquakes in the United States are $5.3 B (FEMA, 2008). From 2000 – 2009, earthquakes killed more people globally than other natural disasters. From 1980 – 2009, six of the seven natural disasters with the largest economic impact were earthquakes (OFDA/CRED, 2009). In the 21st century earthquakes are expected to kill 1.9 – 3.2 million people globally (Holzer and Savage, 2013). Mitigating the effects of earthquakes requires an understanding of earthquake potential, how seismic waves propagate and are attenuated by regional geology, and how the ground behaves locally. In addition, knowledge about the long term history of fault motion can be used to anticipate future activity. These factors are used to estimate probable ground motion and are combined with structural response to evaluate earthquake hazard (Figure 4).

Seismology measures earthquakes as they occur, providing information about the size of the event and its rupture dynamics. Geology measures the long-term effects of earthquakes. Geodesy and topographic imaging contribute by measuring both transient and permanent deformation and the associated spatio-temporal patterns of the earthquake process. GPS data in particular contribute an increasingly important component of the US National Probabilistic Seismic Hazard Maps (Petersen et al., 2014) by mapping the active and ongoing interseismic strain that is the prelude to earthquakes. The latter two provide a means of capturing seismic and aseismic motions that can be compared to long-term and seismological measurements to better assess earthquake risk and reduce uncertainty on the estimates of partitioning between co- and aseismic motions.

Topographic and geodetic imaging measurements are used to:

1. Measure patterns and distribution of fault zone deformation.
2. Determine material properties and relative strength across earthquake fault zones.
3. Understand how fault zone asymmetries and discontinuities affect earthquake ruptures.
4. Respond to earthquake surface ruptures and associated ground failure, landsliding, and damage to infrastructure.

Advances Require Sub-Meter Topography of Active Faults Globally

Key Measurement Requirement: *Transient and Permanent Deformation*

Globally, earthquakes rupture the land surface about 2–5 times per year, typically in earthquakes greater than M6–7 (Table 1, Wells and Coppersmith, 1994). Earthquakes >M7.5

can have postseismic motions that are typically >0.1 m (average from literature search by Donnellan). Earthquakes occurring during the course of a mission provide the opportunity to observe fresh ruptures, and en echelon surface cracking that varies along the length of a rupture zone (Figure 5). Significant individual features along fault ruptures are evident at the decimeter to ten-meter scale and fault slip amounts are similar, driving a resolution requirement of ~0.5 m for large earthquakes (Figure 6).

The field of view, or observable width across a fault zone or single frame, should be on the order of 10 km. Faults consist of a central core on the order of 100 m wide and are surrounded by a damage zone that can be 2 km wide (Ben-Zion and Sammis, 2003). Faulting becomes more complex in the shallow crust and parallel fault strands can be five km apart. The field of view of an instrument should be large enough to capture an entire fault zone. A notional fixed-point imager could collect ≥18,000 linear km of fault zones even with 50% cloud cover and a small 2 km along track field of view (Table 2). Our analysis suggests that a framing camera would complement current pushbroom imagers. Pushbroom imagers are better for simultaneous multispectral imaging over a wider field. 2D framing inherently provides a rigid 2D camera model and lends itself to superior 3D reconstruction compared to a pushbroom, which synthesizes the 2nd dimension with time and is subject to line-of-sight disturbances. Approximately 15 images collected over a range of angles of about ±50° would result in equivalent vertical and horizontal resolution and the ability to resolve features on steep slopes. Additionally, a fixed-point imager would enable short-term change detection or video as the instrument would stare at a particular spot during 2-3 minute pass.

Detecting fault zones as sharp contrasts in geological material, lineaments in soils and vegetation and the presence of seeps and springs drives a need for color imagery draped over the topographic measurements (Figure 7). A damage zone of fault gouge or breccia is formed due to movement on faults, this can be a conduit for ground water, chemically altering the crushed rock. The most prevalent alteration seen is the oxidation of iron from the ferrous state to the ferric state with diagnostic spectral absorption features in the visible-near infrared part of the spectrum (Hunt et al., 1971). Vegetation can be unusually present, absent, or stressed along fault zones. Blockage of groundwater flow against a fault due to the presence of an impermeable barrier typically manifests itself as an oasis in arid terrains or as lines of vegetation in an otherwise vegetation-sparse environment (e.g. Warner and Hendrix 1984). The restriction in groundwater availability also can lead to stressed vegetation.

Surface processes respond to relief produced by recurrent surface rupture on faults. The fine scale of drainage networks ranges from 1-10 m, defining observational requirements. Not only is there value in the characterization of single earthquake ruptures in the near field with topographic differencing (e.g., Oskin, et al., 2012 and Nissen, et al., 2014), but also the longer term record of repeated surface rupture and surface process response is manifest in the spectacular landscapes developed along fault zones. We can assess the evolution of fault zone structure, and distribution of deformation across fault zones with the tools of tectonic geomorphology including topographic metrics (topographic derivatives, drainage network properties, relief, spectral and wavelet analyses; e.g. Hilley and Arrowsmith, 2008; Hilley, et al., 2010; DeLong, et al., 2010). In general, geomorphologists want meter postings of decimeter vertical measurement of changing topography, with opportunity to respond to events, and automated analysis and feature detection (Dieterich, 2009).

Characterizing Earthquake Faults is Imperative for Reducing Risk

Likelihood of Achieving Measurements in Decadal Timeframe: *High*

NASA's geodetic imaging GPS and InSAR measurements provide crustal deformation observations that are invaluable to understanding active faults. Measurement of crustal deformation from continuous GPS is mature where geodetic networks currently exist. Spaceborne InSAR from international satellites provides detail of deformation and damage associated with earthquakes. NASA/ISRO's NISAR mission should launch by 2022. Airborne UAVSAR is an excellent regional and response tool and should continue to fly.

NASA's Earth Venture Suborbital program provides an excellent opportunity for combining UAVSAR and a topographic imager.

Airborne topographic imaging is being developed and adopted by the research community. Small Uninhabited Aerial Vehicle (sUAV) are being used to develop and demonstrate the methodology, while at the same time creating valuable science data products. Small UAVs might readily respond to earthquakes in order to capture immediate fault rupture characteristics and details of postseismic motions. Topographic imaging using a gimbaled instrument or steering mirror could be flown on an airborne platform as part of an Earth Venture Suborbital mission. Coupling UAVSAR and a topographic imager would allow for crustal deformation and surface morphology to be collected simultaneously. Topographic imaging has excellent spaceborne potential and could be flown as an Earth Venture Mission (Figure 8). Similar platforms, such as Worldview, Pleiades, or Terra Bella, would provide complementary and in some cases supplementary measurements. Worldview and Pleiades can provide meter scale topography from photogrammetry. Terra Bella is a small satellite with 10s of cm aperture providing approximately meter imagery and video. Planetlabs fly cubesats with 9 cm aperture delivering 4m imagery.

Spaceborne geomorphic measurements could be used to respond to earthquakes that cause loss of life or property from the mainshock, aftershocks, and associated hazards rapidly and directly. Information during disasters is essential for emergency planners to allocate resources for response and recovery efforts. Scientifically the measurements would enable the monitoring of rapid post-seismic response and evolution of fault zones following large ruptures filling a key observational gap. The data will help to identify processes that occur in close time-space proximity to large earthquake ruptures. A comprehensive geodetic and topographic imaging program will increase understanding of connections between plate tectonics and earthquake ruptures (Figure 9).

Topographic/Fixed-Point Imaging Would Serve a Wide Range of Science Applications

Topographic and fixed-point imaging applies to numerous applications including earthquakes, landslides, volcanoes, coastal erosion, glaciers, sea ice, or river ice breakup. In 2014 the Keck Institute for Space Studies hosted a workshop to study the potential uses of this type of measurement. The resulting report *Gazing at the Solar System: Capturing the Evolution of Dunes, Faults, Volcanoes, and Ice from Space* (Donnellan et al, 2015) recommended frequent high-resolution measurements of shape, spectra, and reflectance of Earth's changing surface in targeted areas around the globe. From these measurements morphology, flux, variability, dynamics, composition, and energy could be derived for a broad set of science applications. Topographic change can provide measurement of volumetric change, such as for glaciers, coastal erosion, landslides, or volcanoes. If the instrument carries a framing camera to derive the 3D structure, then targets would have a 2-3-minute dwell time during a single pass. If so, then short-term rapid changes could be measured and video of the phenomenon would be captured. Rapid dynamic changes could come from lava flows, tsunami, ice bergs, or river ice. Event driven and continuous processes could be observed.

The report states: "*A substantial strength of the gazing approach is that coarse and fine structure, material properties, and surface reflectance can be simultaneously measured. This allows for separation of forcings and deeper understanding for a variety of processes.* ***Recommendation 1:*** *The applications and benefits of gazing imaging should be considered in the upcoming National Research Council Earth Science Decadal Survey. Because the range of applications is so broad, a gazing imaging system would make an excellent facility-type instrument for diverse studies.*"

References

Ben-Zion, Y. and C. G. Sammis, 2003. Characterization of Fault Zones, Pure Appl. Geophys., 160, 677-715.

Ben-Zion, Y., Shi, Z., 2005. Dynamic rupture on a material interface with spontaneous generation of plastic strain in the bulk. Earth Planet. Sci. Letters, 236, 486– 496.

DeLong, S., Hilley, G.E., Rymer, M., Prentice, C., 2010. Fault zone structure from topography: Signatures of en echelon fault slip at Mustang Ridge on the San Andreas Fault, Monterey County, California. Tectonics, 29, TC5003, doi:10.1029/2010TC002673.

DeLong, S.B., Donnellan, A., Ponti, D.J., Rubin, R.S., Seitz, G., Schwartz, D.P., Prentice, C.S., Dawson, T.E, Lienkaemper, J.J., Hudnut, K.W., Rosa, C., Pickering, A., Parker, J.W., submitted. Tearing the terroir: Details and implications of surface rupture and deformation from the 24 August 2014 M6.0 South Napa earthquake, California.

dePolo, C.M., 2008, Quaternary Faults in Nevada, Nevada Bureau of Mines and Geology Special Map 167, D. Meeuwig and J. Price, editors.

Dieterich, W., 2009, Monitoring of Geomorphic processes: fluvial geomorphology, continental erosion, Presentation at the Keck Institute for Space Studies Workshop Monitoring Earth Surface Changes from Space, October 28-30, 2009, Pasadena, California, http://kiss.caltech.edu/workshops/surface2009/schedule.html.

Dokka, R.K. and C.J. Travis, 1990, Role of the eastern California Shear zone, Geophys. Res. Lett., v.17, n. 9, p. 1323-1326.

Donnellan, A., Glasscoe, M., Abrams, M., Rundle, J., Arrowsmith, J.R., Ben-Zion, Y., Goguen, J., A. Ansar, A., Burl, M., 2014. Assessing Earthquake Hazard from Relationships between Fault Zone Morphology and Rupture Characteristics. White paper submitted to the 2017 Earth Science Decadal Survey.

Donnellan, A., Hallet, B., Leprince, S., study leads, 2015. Gazing at the Solar System: Capturing the Evolution of Dunes, Faults, Volcanoes, and Ice from Space. Report of the Keck Institute for Space Studies Workshop, June 16 – 20, 2014, California Institute of Technology, 54 pp.

Dor, O., Yildirim, C., Rockwell, T.K., Ben-Zion, Y., Emre, O., Sisk, M., Duman, T.Y., 2008. Geological and geomorphologic asymmetry across the rupture zones of the 1943 and 1944 earthquakes on the North Anatolian Fault: possible signals for preferred earthquake propagation direction. Geophys. J. Int., 173, 483–504.

FEMA, 2008. HAZUS® MH Estimated Annualized Earthquake Losses for the United States, 53 pp.

Hilley, G.E., Arrowsmith, J.R., 2008. Geomorphic response to uplift along the Dragon's Back pressure ridge, Carrizo Plain, California. Geology, 36, 5, 367-370; doi: 10.1130/G24517A.1.

Hilley, G.E., Prentice, C.S., DeLong, S.B., Blisniuk, K., Arrowsmith, J.R., 2010. Morphologic dating of fault scarps using airborne laser swath mapping (ALSM) data. Geophysical Research Letters, 37, L04301, doi:10.1029/2009GL042044.

Holzer, T.L., Savage, J.C., 2013. Global Earthquake Fatalities and Population. Earthquake Spectra, 29, 155-175.

Hunt, G.R., Salisbury, J.W., Lenhoff, C.J., 1971. Visible and near infrared spectra of minerals and rocks. III. Oxides and hydroxides. Mod. Geology, 2, 195-205.

Johnson, K., Nissen, E., Saripalli, S., Arrowsmith, J.R., McGarey, P., Scharer, K., Williams, P., Blisniuk, K., 2014. Rapid mapping of ultra-fine fault zone topography with Structure from Motion. Geosphere, 10, 5, 1-18. doi:10.1130/GES01017.1.

Kagen, Y.Y., Jackson, D.D., Geller, R.J. 2012. Characteristic Earthquake Model, 1884–2011, R.I.P. Seism. Res. Lett., 83, 951–953, doi: 10.1785/0220120107.

OFDA/CRED International Disaster Database, 2009. (www.emdat.be), Université catholique de Louvain Brussels – Belgium. Summarized by International Strategy for Disaster Reduction (UNISDR) and Centre for Research on the Epidemiology of Disasters (CRED), Department of Public Health, Université catholique de Louvain, Belgium.

Olsen, K.B., Day, S.M., Minster, J.B., Cui, Y., Chourasia, A., Faerman, M., Moore, R., Maechling, P., Jordan, T., 2006. Strong shaking in Los Angeles expected from southern San Andreas earthquake. Geophys. Res. Lett., 33, L07305, doi:10.1029/2005GL025472.

Petersen, M.D., Zeng, Y., Haller, K.M., McCaffrey, R., Hammond, W.C., Bird, P., Moschetti, M., Shen, Z., Bormann, J., Thatcher, W., 2014. Geodesy- and geology-based slip-rate models for the Western United States (excluding California) national seismic hazard maps. U.S. Geological Survey Open-File Report 2013–1293, 80 p., http://dx.doi.org/10.3133/ofr20131293.

Rodgers, D.W. and Little, T.A., 2006. World's largest coseismic strike-slip offset: The 1855 rupture of the Wairarapa Fault, New Zealand, and implications for displacement/length scaling of continental earthquakes. Journal of Geophysical Research: Solid Earth, 111(B12).

Thatcher, W., G.R. Foulger, B.R. Julian, J.Svarc, E. Quilty, G.W. Bawden, 1999, Present-day deformation across the Basin and Range Province, Western United States.

Warner, R.E., Hendrix, K.M., 1984 (eds.). California Riparian Systems: Ecology, Conservation, and Productive Management. Berkeley. University of California Press, 1984. http://ark.cdlib.org/ark:/13030/ft1c6003wp/.

Wechsler, N., Rockwell, T.K., Ben-Zion, Y. 2009. Application of high resolution DEM data to detect rock damage from geomorphic signals along the central San Jacinto Fault. Geomorphology, 113, 82-96.

Wells, D., Coppersmith, K., 1994. New Empirical Relationships among Magnitude, Rupture Length, Rupture Width, Rupture Area, and Surface Displacement. Bull. Seism. Soc. Am., 84, 974–1002.

Wesnousky, S.G., 2005. The San Andreas and Walker Lane fault systems, western North America: Transpression, transtension, cumulative slip and the structural evolution of a major transform plate boundary. Journal of Structural Geology, 27(8), pp.1505-1512.

Figures

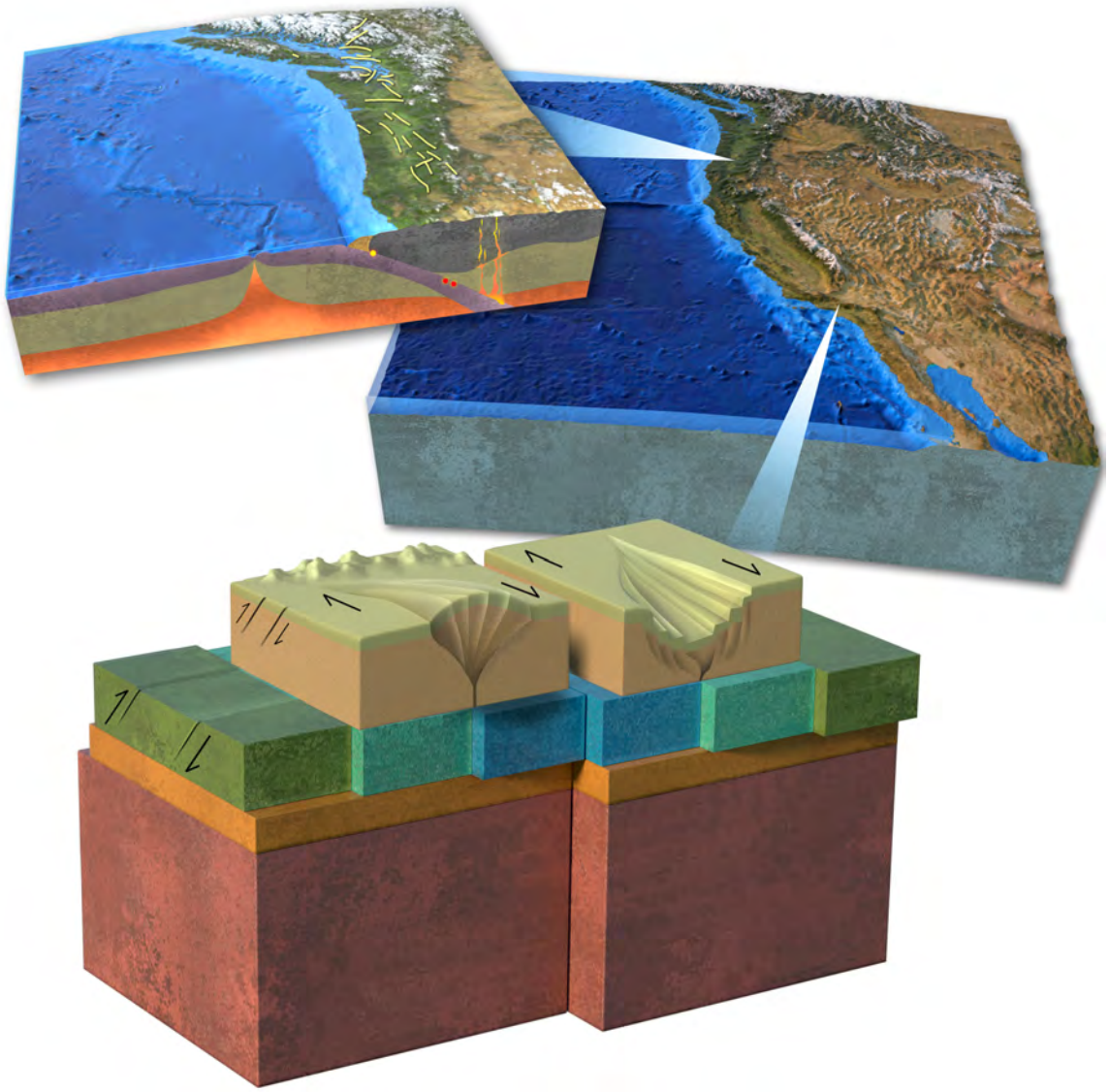

Figure 1. Western United States showing how strike-slip, thrust, and subduction plate boundaries might connect to faults at the surface. The faults could connect hierarchically from a simple mantle boundary to a complex fault system at the surface (artwork Chuck Carter, Jet Propulsion Laboratory).

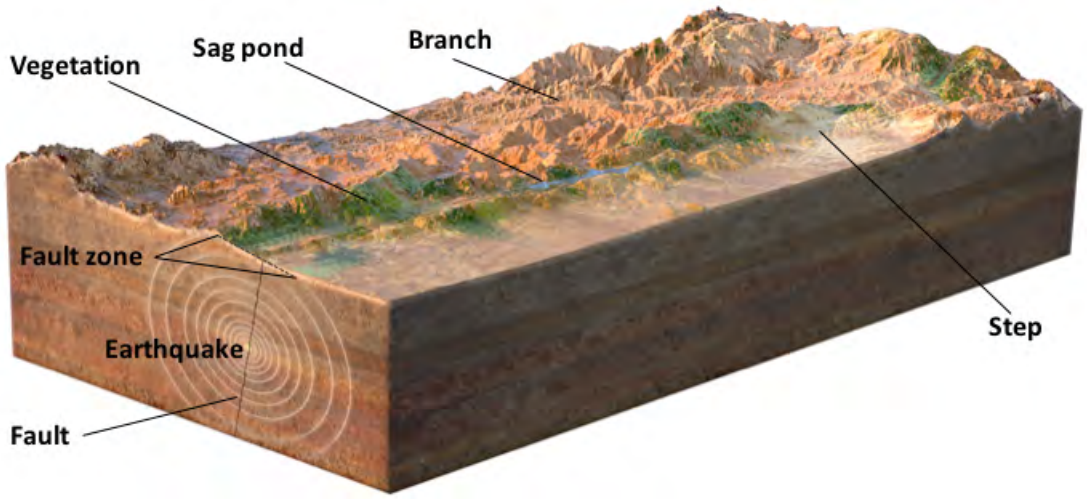

Figure 2. Faults are made up of a central core surrounded by a damage zone. Key topographic features observable at the surface provide information about the width of the fault zone, the roughness of the fault, and the orientation of the fault relative to tectonic motions (artwork Chuck Carter, Jet Propulsion Laboratory).

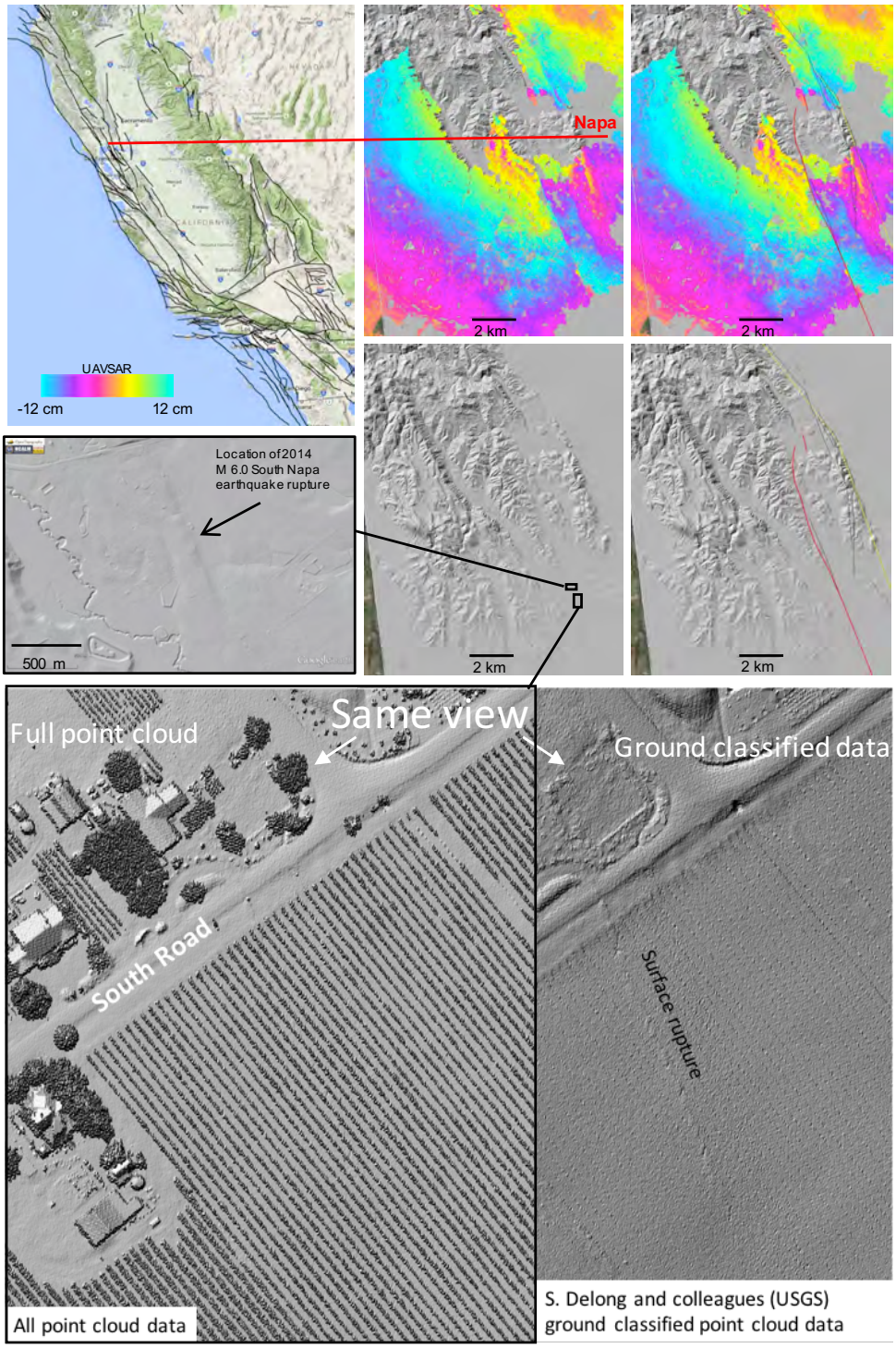

Figure 3. UAVSAR and topographic images of the region of the 2014 M6.0 South Napa earthquake. Upper: The two right UAVSAR and lidar panels show the data with and without the ground rupture. The area of no data in the UAVSAR image is due to decorrelation between the before and after pairs of images. The earthquake ruptured a bench that appears in lidar data from before the earthquake but 5 km west of the fault trace that was mapped as active. Lower: Left: disruption of vineyard is not evident in the full point cloud. Right: Ground classified lidar data from left image highlight the decimeter-scale surface rupture.

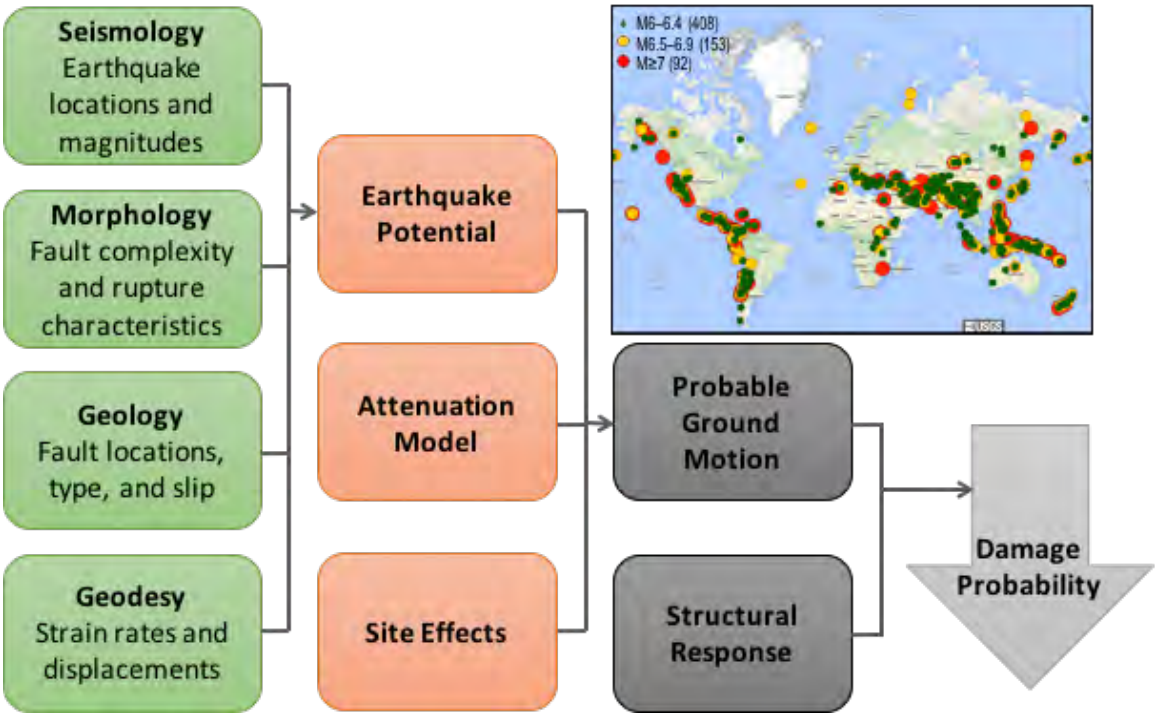

Figure 4. Flow from science and observations to earthquake hazard assessment. Upper right map shows the locations of large earthquakes from 1970–2015. There were 245 M≥6.5 earthquakes in that time frame with 92 of them M≥7.

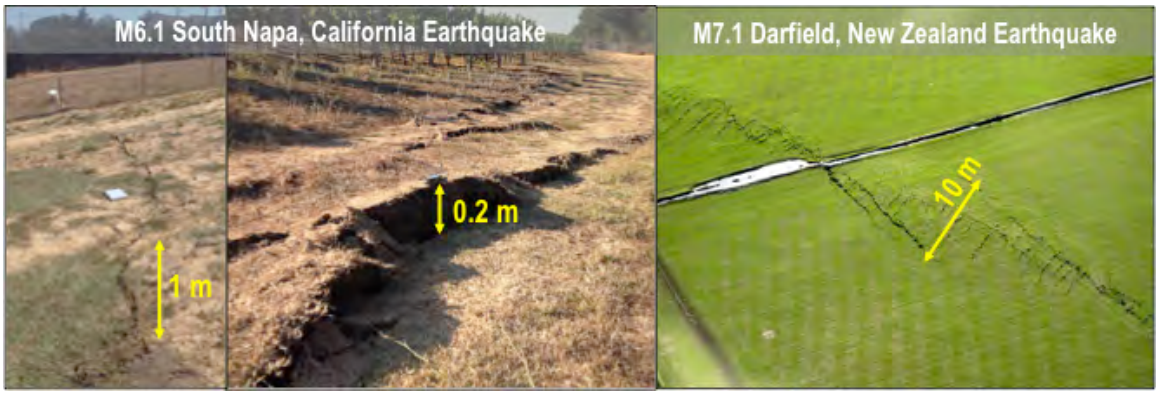

Figure 5. Features found in fault zones after earthquakes occur. Left: surface cracking from the 2014 M6 South Napa earthquake. Middle: en echelon fractures in the fault zone. Right: Surface cracking associated with the 2010 M7.1 Darfield earthquake that devastated Christchurch, New Zealand. Note the variable width of this fractured zone along the length of the fault.

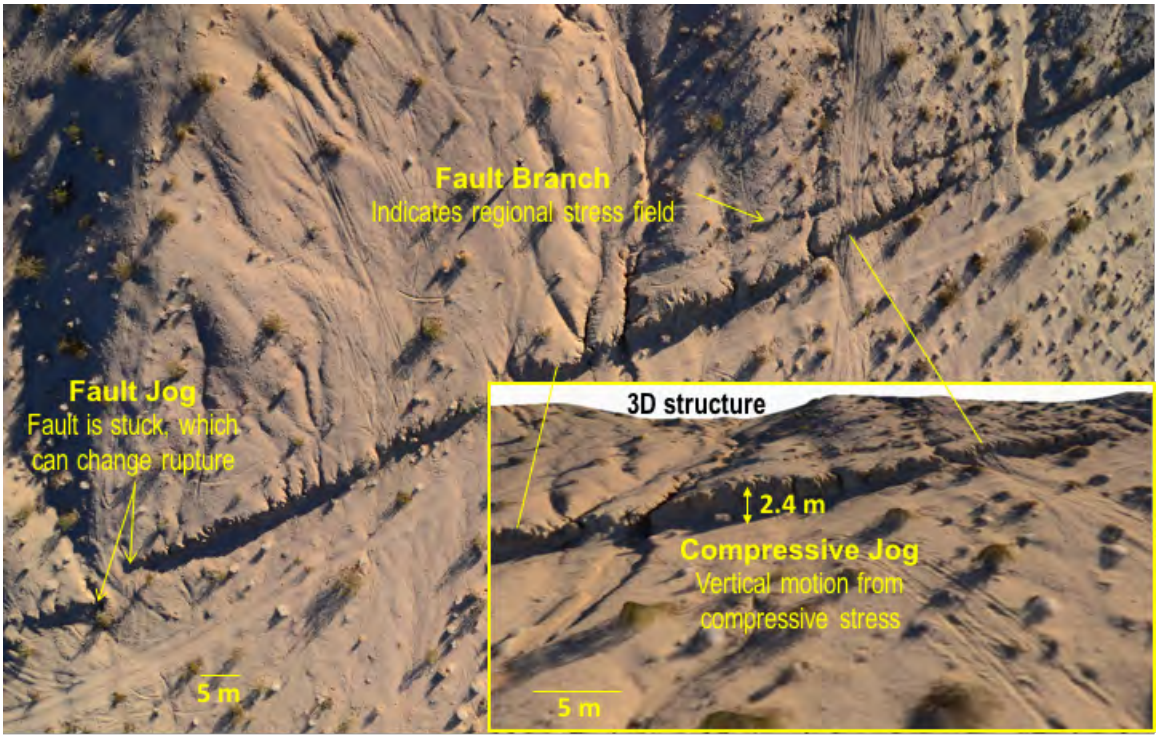

Figure 6. 3D reconstruction from images collected from a balloon of the 1992 M7.2 Landers earthquake rupture in California. Observations were collected at 60 m above ground using a Nikon D5100. Features can be identified that provide information about the fault rupture, roughness, and stress field. (see also Johnson, et al., 2014).

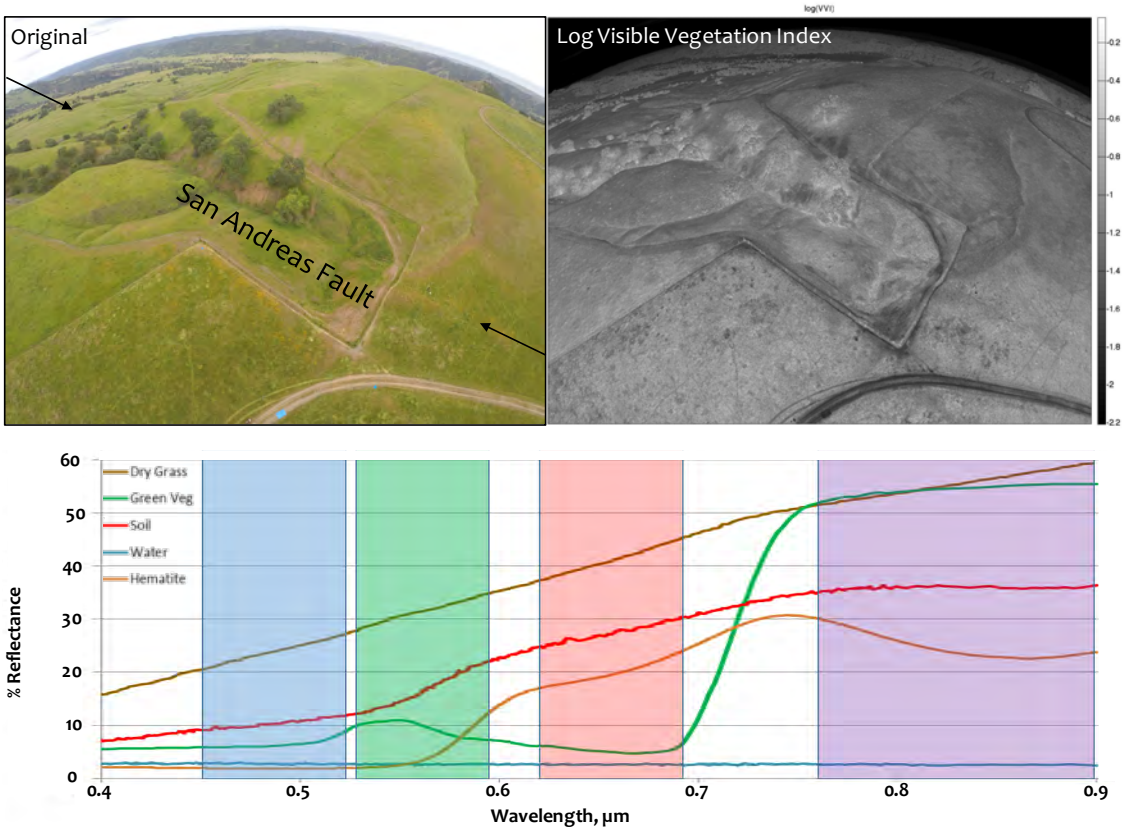

Figure 7. Example small UAV (sUAV) image of the creeping section of the San Andreas fault. Upper right shows the log of visible vegetation index extracted from the image. Sub-meter resolution color products recover characteristics of active fault zones. Four colors are sufficient to discriminate key compositional boundaries. Four proposed VIS-NIR bands can identify compositional boundaries of key fault zone materials.

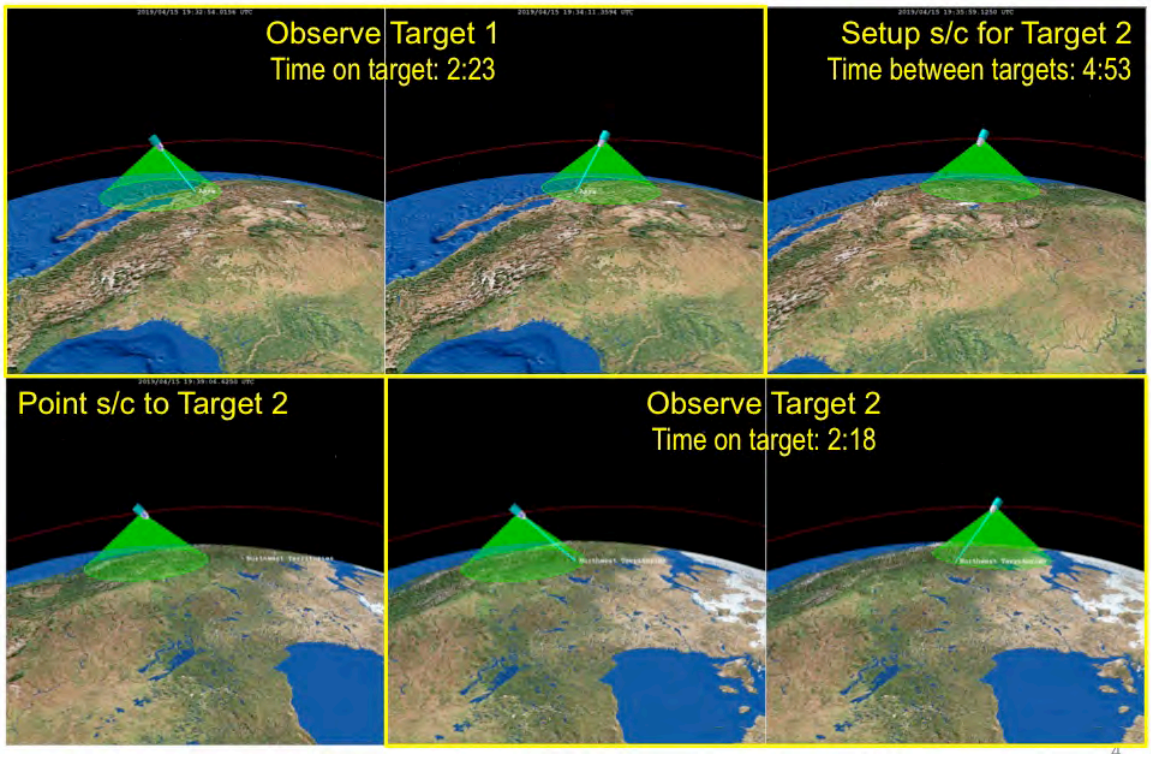

Figure 8. Measuring fault zone morphology requires multi-angle imaging of a target for 3D reconstruction of topography and determination surface cracking and fault zone damage. Such a system would dwell on a target for minutes during a pass before moving on to the next target.

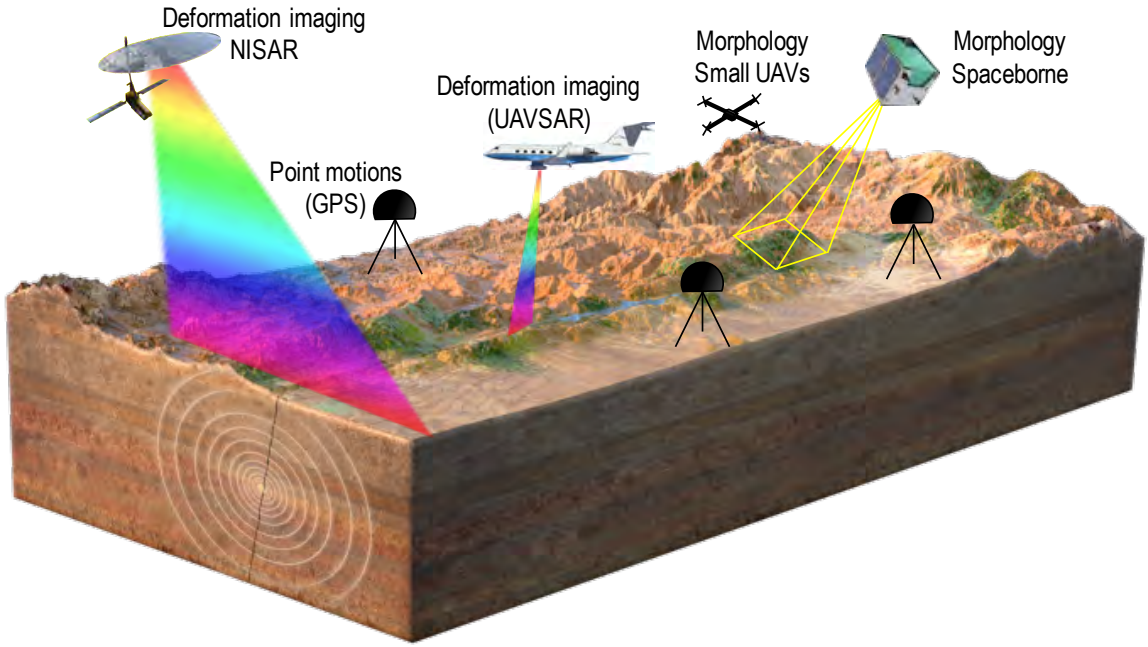

Figure 9. Connecting plate boundary processes to earthquake fault behavior requires a comprehensive program of geodetic and topographic imaging. This would provide broad sampling of the spatio-temporal behavior of tectonic and fault zones including short-term transient deformation and long-term permanent deformation (artwork Chuck Carter, Jet Propulsion Laboratory).

Tables

Table 1. Values for key parameters of 129 continental surface rupturing earthquakes (left; from Wells and Coppersmith, 1994) and postseismic motion observed for earthquakes globally (right; literature search by A Donnellan). *M8.1 Wairarapa earthquake (Rodgers and Little, 2006).

Coseismic	Ave.	Min.	Max.	Postseismic	Ave.	Min.	Max.
Magnitude (land surface rupturing earthquakes)	Mw 6.7 Ms 6.8	Mw 5.2 Ms 4.6	Mw 8.1 Ms 8.5	Magnitude (globally including oceans)	7.5	6.0	9.5
Surface rupture length	56km	1.3 km	432km	Slip	6 m	1m	20m
Maximum slip for single fault rupture	2.7m	0.02 m	14.6m 18.7m*	Postseismic slip	0.8m	0.1m	2m
Average slip displacement along fault per rupture	1. m	0.05 m	8m	% of postseismic slip versus coseismic slip	55%	0%	300%

Table 2. Data sufficiency for a notional 2-year mission with a framing camera. Push-framing or other instrument designs may allow a larger field of view.

Assumptions	M≥6.5 earthquakes	M≥7 earthquakes
25 targets per day	250 fault zones (245 land earthquakes 1970–2015)	100 km fault zones (92 land earthquakes 1970–2015)
2 year mission	50 km average rupture length	100 km average rupture length
2 km x 2 km field of view	**Need:** 12,500 km total rupture length	**Need:** 10,000 km total rupture length
36,500 linear km total	75 km average rupture length	
18,250 linear km observed with 50% cloud cover	**Need:** 19,375 km total rupture length	